BLINKING CHARACTERISTICS OF ORGANIC FLUOROPHORES FOR BLINK-BASED MULTIPLEXING

Amelia G. Seabury, Alisha J. Khodabocus, Isabelle M. Kogan, Grayson R. Hoy, and Grace A. DeSalvo
Advisor: Kristin L. Wustholz
William & Mary, Department of Chemistry, P.O. Box 8795, Williamsburg, VA 23187

ABSTRACT

To deepen our understanding of both biological and material systems for NASA-relevant research, visualization of the complexity occurring on the nanometer scale is critical. Multicolor single-molecule fluorescence studies allow for a nuanced understanding of intricate structures within cells, nanomaterials, and polymers but are limited by the necessity of spectrally distinct probes or time intensive procedures. Recently, we demonstrated an alternative method termed blink-based multiplexing (BBM) wherein spectrally-overlapped emitters are classified based solely on their blinking dynamics (i.e., fluctuations in emission intensity under constant excitation caused by intrinsic photo-physical or -chemical transitions). This study parses the relationships between structure and blinking activity of rhodamine, BODIPY, and anthraquinone fluorophores to ultimately optimize BBM performance. Through change point detection and multinomial logistic regression analyses, we show that BBM can harness differences in spectral diffusion, charge transfer kinetics, and photostability to distinguish and accurately classify fluorophores. Informed by their photo-physical or -chemical properties, BBM can simultaneously differentiate groups of 2 or 3 spectrally-overlapped emitters using a single laser with ≥ 93% accuracy.

INTRODUCTION

Single-molecule spectroscopy (SMS) experiments reveal the heterogeneity of molecular behavior previously hidden behind ensemble averaging.[1–3] Not only can valuable information be gleaned from single molecules "nanoreporting" on their environment, but these measurements also led to the groundbreaking development of single-molecule localization microscopy (SMLM).[4–6] In this technique, photoexcited fluorescent probes stochastically fluctuate between emissive 'on' states and non-emissive 'off' states in a phenomenon known as blinking. A controlled subset of molecules blink 'on' at a given time and their position can be localized so that a "super-resolved" image down to tens of nanometers can be developed over many blinking cycles.[4–7]

Although SMLM techniques yield nanoscale resolution, the multicolor imaging necessary to illuminate complex NASA-relevant systems so that scientists and engineers can control and leverage their function has proven challenging. A straightforward technique is to use fluorescent probes with spectrally-distinct emission (e.g., red, green, and blue fluorescent dyes). However, there are a limited number of probes of different colors that operate effectively together, and additional issues caused by spectral overlap can arise.[4,6] While the need for spectrally-distinct probes can be avoided with sequential labeling and imaging approaches, these methods are time intensive.[4,6]

In 2022, the Wustholz lab demonstrated a rapid, accurate multicolor technique named blink-based multiplexing (BBM).[8] Whereas former techniques leveraged blinking to localize molecules, BBM seeks to classify and false-color multiplex emitters by quantifying their blinking dynamics under constant excitation of a single laser. The advantages of BBM are that the detection of distinct emitters is simultaneous, it uses a single excitation wavelength, and it does not rely on probe color for detection. In the initial proof-of-concept study, the two model emitters, rhodamine 6G (R6G) and CdSe/ZnS quantum dots (QD), were successfully differentiated and multiplexed with an accuracy >93% using both empirically-derived metrics and deep learning algorithms.[8] Recently, BBM of the aforementioned emitters was also demonstrated at varying excitation powers and experimental bin times, as well as in a poly(vinyl alcohol) environment.[9]

These experiments confirmed the feasibility of BBM and identified optimal BBM conditions for the QD/R6G system, but several questions remain unanswered. First, it is important to determine if BBM can differentiate between biocompatible organic fluorophores (e.g., rhodamines) for future applications in biological systems.[7,10] Second, the effect of emitter structural, photophysical, and photochemical properties on BBM performance is currently unexplored and could contribute to selecting more effective BBM systems. To take full advantage of the BBM method, which holds the promise to significantly expand the palette of available fluorescent probes for SMLM, this study addresses the two above knowledge gaps.

First, we study the blinking dynamics and BBM performance of five spectrally-overlapped rhodamine probes: 5-carboxy-X-rhodamine (5ROX), rhodamine 123 (R123), rhodamine 560 (R560), rhodamine 6 G (R6G), and rhodamine B (RB). These fluorophores have been shown to share a blinking mechanism of dispersive electron transfer (ET) to and

from trap states on glass.[11–13] Both a shared blinking mechanism and a broad distribution of on and off events caused by dispersive ET should hinder BBM and test the limits of this method. However, structural differences in selected rhodamines result in varying flexibility, polarity sensitivity, N-dealkylation, and ET kinetics that can allow for blink-based classification despite other similarities.[7,14–16] Indeed, we observe that BBM can distinguish between pairs of rhodamines with ≥ 90% accuracy at the price of some data loss.

Next, we examine probes of different molecular classes, namely pyrromethene 605 (PM605) and alizarin (AZ) via BBM. The former falls in the dipyrromethene (BODIPY) family and has an unknown blinking mechanism, and the latter is an anthraquinone which experiences excited-state intramolecular proton transfer (ESIPT).[17] Furthermore, we study QDs, which undergo dispersive charge transfer processes unique from the rhodamine dyes.[18,19] As anticipated, differences in blinking mechanism and ET kinetics cause increased BBM accuracy and data retention which allows for effective two- and three- color multiplexing. Overall, this study not only reveals the fundamental connections between emitter structure and blinking, but also harnesses this information for BBM.

METHODS

Materials, Sample Preparation, Emission Spectroscopy

R6G (Acros Organics, 99%), R123 (Acros Organics, 99+%), 5ROX (5-carboxy-X-rhodamine, triethylammonium salt, ThermoFisher Scientific), RB (Acros Organics, 99%), R560 (Exciton), QD (Invitrogen, Qdot 565 ITK carboxyl quantum dots, 8 μM solution in borate buffer), AZ (Acros Organics 97%), and PM605 (Exciton) were used as received. Using base bathed glassware (1M KOH for 12-24 h), stock solutions of QD, R6G, R123, 5ROX, RB, and R560 were prepared in Type 1 ultrapure water (Thermo Scientific, Easy Pure II, 18.2 MΩ cm) while the AZ and PM605 stock solutions were prepared in ethanol (absolute anhydrous, 200 proof). Prior to use for single-molecule experiments, stock solutions were briefly sonicated and diluted to ~1 nM in their respective solvents. Glass coverslips were prepared by base bathing for 12-24 h, rinsing with ultrapure water, and drying with clean air (Wilkerson, X006-02-000). A 35 μL aliquot of the diluted solution was spin coated (Laurell Technologies, WS-400-6NPP-LITE) onto a glass coverslip at 3000 rpm for 30 seconds with a 5 second acceleration time. Bulk emission spectra were collected with a spectrofluorometer (FS5, Edinburgh Instruments) using 10^{-5}-10^{-6} M [dye] in 1 cm quartz cuvettes. The excitation wavelength was set to 532 nm and emission was scanned from 535 to 700 nm with a 1 nm step and a 0.1 s dwell.

Single-Molecule Microscopy

Samples were affixed to a custom aluminum flow cell (approx. 1.5 x 3 x 0.5 in.), flushed with dry N_2 via Tygon tubing before and during each experiment (Key Instruments, MR3A01AVVT, approx. 0.2-0.5 scfh) and set on a nanopositioning stage (Physik Instrumente, LP E-545) on an inverted confocal microscope (Nikon, TiU). Laser excitation (Spectra Physics, Excelsior, 532 nm) with a power of ~1 μW was focused to a diffraction-limited spot utilizing a high numerical aperture (NA) 100× oil-immersion objective (Nikon Plan Fluor, NA = 1.3). Emission from the sample was passed back through the objective, a long pass edge filter (Semrock, LP03-532RS-2S) to an avalanche photodiode detector (APD) with a 50 μm aperture (MPD, PDM050CTB) to achieve confocal resolution. A z-axis microscope lock (Applied Science Instruments, MFC-2000) was used to ensure the laser stayed in focus during raster scans. To both control the nanopositioning stage and collect ~10 x 10 μm² emission micrographs over a 30 ms integration time, a custom LabView program was used. The blinking dynamics of single emitters were observed for 100 s for AZ (n=146) and 150 s for QD (n=143), PM605 (n=116), 5ROX (n=95), RB (n=71), R560 (n=64), R123 (n=132), and R6G (n=148) with a 10 ms dwell time. For BBM studies with AZ, QD (n=143), PM605 (n=116), 5ROX (n=135), RB (n=71), R560 (n=64), R123 (n=133), R6G (n=148) were truncated to match the 100 s AZ traces. To determine the presence of single emitters, the concentration dependence of the spot density, blinking dynamics, and irreversible single-step photobleaching of diffraction limited spots were observed.

Blinking Analysis and Emitter Classification

Based on the approach by Yang and coworkers, the method of change point detection (CPD) was employed to quantify statistically significant emission intensities (reported in units of counts per 10 ms bin) and respective durations from binned data.[20] The details of this technique are presented by Kopera and coworkers.[13] The lowest deconvolved intensity is labeled as ‘off’, and emissive ‘on’ events have intensities which fall one standard deviation above the rms noise. A total of 10 independent blinking statistics are extracted from each blinking trace and then standardized via z-score normalization.

The identity of the emitter, along with its normalized statistics were then applied to multinomial logistic regression (MLR) analysis in MATLAB. In MLR, the probability of a molecule being class A (P_A)

is first fit to a log-likelihood (sigmoid) function shown by **Equation 1**. The resulting fit parameters are output as a linear combination of regression coefficients (*m, n, …*) with their associated predictor (*x, y, …*) and a vertical intercept (*b*) where the predictors are the 10 independent CPD statistics **(Equation 1)**.

$$P_A = \frac{e^{(m_k x + n_k y + .., b_k)}}{\sum_{k=1}^{K} e^{(m_k x + n_k y + .., b_k)}} \qquad (1)$$

For binary classification, MLR generates one set of regression coefficients, but since there are three classes total (*K=3*) for ternary classification, there are two (*K-1*) total sets of nonzero regression coefficients. The first set of coefficients corresponds to the fit parameters comparing class A to class C (*k=1*), the second set compares class B to class C (*k=2*), and class C is designated as the 'pivot' class with all coefficients set to zero (*k=3*).

Then, with emitter identities removed, each dataset of blinking traces was divided into training (90%) and testing (10%) for 10-fold cross-validation analysis to gauge the model's ability to accurately predict emitter identity. The probabilities resulting from the cross-validation analysis were employed for classification. For binary classification, a default threshold of $P_A > .50$ was used to determine whether an emitter belongs to class A or B and default threshold of $P_A > .33$ was applied to classify emitters into A versus B or C.

RESULTS AND DISCUSSION

BBM of fluorescent rhodamine dyes

To probe the capability of BBM to distinguish fluorophores with a shared blinking mechanism, 5ROX, R123, R560, R6G, and RB were examined. Due to the significant overlap in emission spectra seen in **Figure 1**, these fluorophores would be unsuitable for traditional spectral-based multiplexing. Approximately 100 nm separation is required for spectral differentiation, but these rhodamines have emission maxima which are ≤ 30 nm apart, with the exception of R560 and 5ROX which are 70 nm apart.[21,22] Additionally, RB and R560 were selected as a negative control since RB is known to undergo N-dealkylation to produce R560 when excited at 532 nm. Hence, RB and R560 should not be readily differentiated via BBM as the RB dataset effectively contains R560.[16,23]

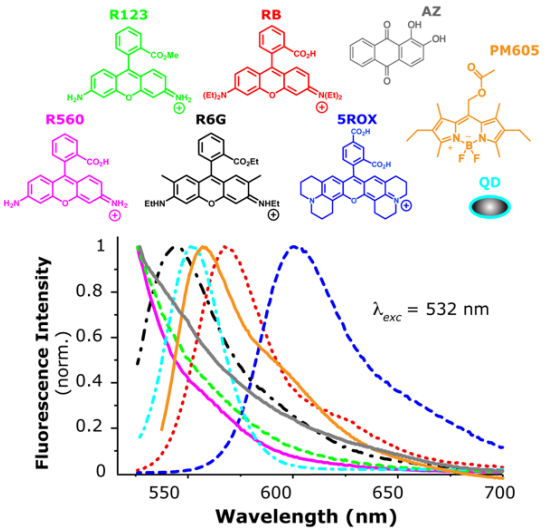

Figure 1: Structures and bulk fluorescence spectra of the probes examined in this study. (pink solid) R560, (green dashed) R123, (black dash-dotted) R6G, (red dotted) RB, (blue dashed) 5ROX, (gray solid) AZ, (cyan dash-dotted) QD, and (orange solid) PM605. Reprinted with permission from reference 24.

To begin, blinking measurements for ~100 molecules of each of rhodamines were collected under the same experimental conditions. Due to the complexity and non-binary nature of the emission-time traces, CPD was used to quantify emission intensities and temporal statistics. Representative blinking traces of 5ROX and R6G are displayed in **Figure 2A and 2B** with CPD analysis visualized as a red line. Quantitatively, CPD also outputs 10 independent statistics: the number of distinct intensities (N_I), minimum and maximum emissive intensities (I_{min} and I_{max}), time-averaged intensity ($\langle I \rangle_t$), average length of on and off segments ($\langle t_{on,seg} \rangle$ and $\langle t_{off,seg} \rangle$), average length of on and off intervals ($\langle t_{on,int} \rangle$ and $\langle t_{off,int} \rangle$), and the number of on and off segments over each trace ($N_{on,seg}$ and $N_{off,seg}$). The temporal CPD statistics are divided into intervals and segments, with segments referring to the amount of time an event remains at a particular intensity and intervals denoting the length of time before switching between on and off events.

To test BBM viability, normalized CPD statistics and emitter identities were input into a MATLAB code for MLR analysis and classification. For the 5ROX/R6G example (where 5ROX is class A and R6G is class B from the general form A/B used throughout the study), the default accuracy output by MLR is 86.4%. The overall classification accuracy can be visually broken down via a confusion matrix where the true identity of the emitter is located on the

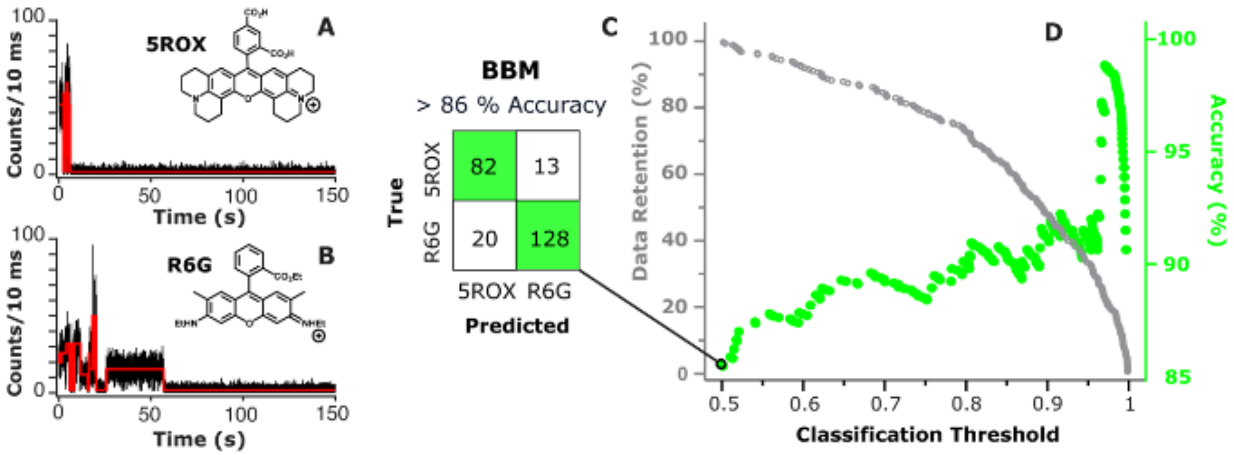

Figure 2: Blinking analysis and MLR-based classification of 5ROX and R6G. Reprinted with permission from reference 24.

y axis and the predicted classification is along the x axis **(Figure 2C)**. In this case, 13 molecules which were truly 5ROX are incorrectly classified as R6G **(Figure 2C)**.

The probability thresholds can be adjusted to optimize classification accuracy by removing "less certain" data.[9] For 5ROX/R6G, when the probability threshold is set to the minimum ($P_A > .50$), the classification accuracy is 86.4%. However, increasing the probability threshold to 0.66 results in an impressive 90% accuracy while maintaining 88% of the blinking data (i.e., 88% of data is retained and the 12% that falls between a P_A of 0.5 and 0.66 is removed). The overall upward trend of classification accuracy as threshold increases and the corresponding loss of data is shown in **Figure 3D**.

Table 1: Binary BBM-based classification results for 5ROX, R123, R560, and RB

Classification	minimum			for 93% accuracy	
	accuracy (%)	TPR	FPR	threshold	data retention (%)
5ROX/R6G	86.4	0.86	0.13	0.97	26
R6G/RB	80.4	0.83	0.31	0.95	28
5ROX/R560	76.1	0.85	0.38	0.92	35
R123/RB	69.5	0.83	0.55	0.87	22
R6G/R123	81.8	0.8	0.17	×	
R6G/R560	71.2	0.87	0.66	×	
R123/R560	69.9	0.86	0.63	×	
5ROX/RB	69.3	0.78	0.42	×	
5ROX/R123	64.3	0.34	0.14	×	
R560/RB	58.5	0.47	0.31	×	

This approach was applied to all binary combinations of the five available rhodamines, as summarized in **Table 1**. Table 1 establishes the wide range of minimum accuracies output by MLR with the most accurately classified pairing being 5ROX/R6G and the least being R560/RB. In fact, the classification accuracy of R560/RB falls just above random guessing (50% accuracy) at 58.5%. This result supports the interpretation that R560 and RB are not readily differentiated due to photoinduced N-dealkylation of RB into R560 and other intermediates.[23] Aside from R560/RB, 6 out of 9 rhodamine pairs can achieve 90% classification accuracy by elevating the probability threshold with retention ranging from above 75% to about 25%. Aiming further to 93% accuracy, 4 of 9 pairs are viable, albeit with relatively low data retention **(Table 1)**. Overall, despite complex blinking dynamics and a shared molecular class, accurate two-color BBM is possible for several rhodamine pairs.

<u>Impact of rhodamine properties on BBM classification</u>

MLR classification determined that 5ROX/R6G, R6G/RB, 5ROX/R560, and R123/RB were the most successful BBM pairs based upon minimum classification accuracy and ability to reach 93% accuracy with thresholding **(Table 1)**. However, a more critical investigation of the MLR fits in association with photophysical and photochemical properties of these fluorophores is necessary to understand these results.

The fit parameters derived from MLR analysis are unique to each classification problem and provide insight into the most important blinking statistics for classification. For example, the highest weighted predictors for the 5ROX/R6G classification problem **(Equation 2)** are I_{min}, $N_{off,seg}$, $\langle I \rangle_t$, and

$N_{on,seg}$. This indicates that these CPD statistics are the most critical for differentiating between 5ROX and R6G.

$$-2.7I_{min} - 0.8N_{off,seg} - 0.7\langle I\rangle_t + 0.6N_{on,seg} + 0.4\langle t_{on,int}\rangle + 0.4I_{max} - 0.4N_I - 0.3\langle t_{on,seg}\rangle + 0.2\langle t_{off,int}\rangle - 0.2\langle t_{off,seg}\rangle - 1.3 \quad (2)$$

Over the 9 pairs of rhodamines, five CPD-derived statistics are most heavily weighted for BBM classification: I_{min}, N_I, $N_{off,seg}$, $\langle t_{off,seg}\rangle$, and $\langle t_{off,int}\rangle$[24]. Hence, both brightness and emission intensity fluctuations (I_{min}, N_I) and the longevity of dark states ($\langle t_{off,seg}\rangle$, and $\langle t_{off,int}\rangle$) are key to effective classification.

According to prior studies, emission intensity can be influenced by brightness, conformational flexibility[15], N-dealkylation,[15,16,23] and molecular environment,[7,14,15] and therefore may be playing a role in I_{min} differentiation. The most straightforward explanation for the relation of I_{min} to rhodamine spectral properties is simply their brightness. However, this would imply that I_{max} would also be a dominant factor in differentiating fluorophores. Since this is not the case, rather than brightness alone, it appears that these "dim" states in particular are crucial to classification. Zhang et al. showed the intensity fluctuations of single molecules of R560, RB, rhodamine 101 (R101, closely related to 5ROX), and other small molecule dyes on glass are connected to significant shifts in emission wavelength.[15] These spectral shifts are rationalized by N-dealkylation, but more dominantly by freedom of their N,N-dialkylated groups to rotate.[15] By this logic, the five rhodamines can be divided into three categories: those that have both N,N-dialkylated rotation and N-dealkylation functionalities (R6G and RB), only N-dealkylation ability (5ROX), and neither (R123 and R560). With the reasoning that rhodamines from different categories would be more easily differentiated, the success of 5ROX/R6G, 5ROX/R560, and R123/RB pairs for BBM is rationalized. However, the distinguishability of R6G and RB remains unclear.

The temporal values $t_{off,int}$ and $t_{off,seg}$ are also key statistics, especially for R6G/RB and R123/RB differentiation, and therefore are valuable to BBM classification.[24] Previous single-molecule experiments utilized on and off interval distributions to examine the photophysical mechanism of on and off switching.[11–13] Specifically, single-molecule studies of rhodamine fluorophores immobilized on glass and TiO_2 produced lognormal distributions of on and off intervals, consistent with the Albery model of dispersive ET kinetics.[25] To elucidate the switching kinetics for the 5ROX, R123, R560, R6G, and RB datasets, complementary cumulative distributions functions (CCDFs), maximum likelihood estimation (MLE) and Kolmogorov-Smirnov (KS) fitting techniques were employed. First, the CCDFs show the likelihood that an event occurs in a time greater than or equal to the time t on the x axis of the function.[12,26] Then, MLE/KS analysis of these broad, heavy tailed distributions reveal that lognormal distributions most accurately represent the CCDFs over other test functions, aligning with the Albery model as expected.

Although all five rhodamines fit lognormal distributions, the differences (and similarities) in fit parameters provide insight to the specific switching dynamics of each fluorophore. The on-interval CCDFs are highly overlapped, with a median (μ_{on}) and standard deviation (σ_{on}) of the distribution corresponding to ~0.01 and ~1.9 respectively **(Figure 3A)**. Hence, ET kinetics to dark states cannot appreciably contribute to distinguishability of the selected rhodamines. On the other hand, the off-interval CCDFs show considerable differences in lognormal fits with μ_{off} values of –1.3, -1.27, -0.7, -0.3, and –0.1 corresponding to 5ROX, R6G, R560, RB, and R123.[24] Since the average rate constant for back kinetics is proportional to $-\mu_{off}$ according to the Albery model, the average dark state decay rate constants follow the order 5ROX ~ R6G > R560 > RB > R123.[11,13] Further, σ_{off} values range from 2.0 to 2.6, with the lowest value corresponding to 5ROX and the highest for RB.[24] The σ_{off} values correlate to the dispersion about the average back ET rate constant, which implies that 5ROX has minimal dispersion and RB has the most significant amount of dispersion about μ_{off}. The high recombination dispersion of RB is logical given that the fluorophore can undergo both N,N-dialkylated rotation and N-dealkylation.

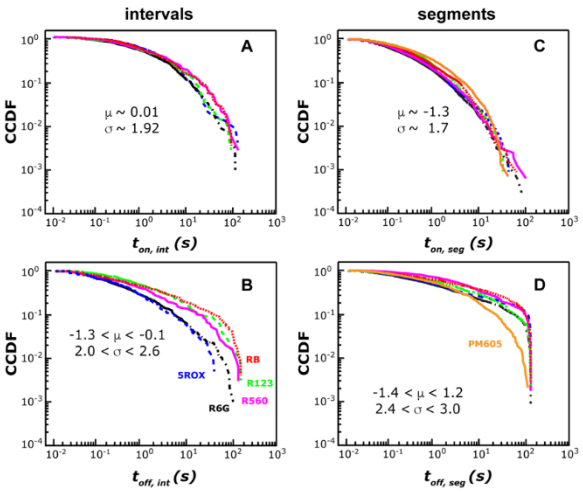

Figure 3: Distributions of blinking event durations for 5ROX, R123, R560, R6G, RB, and PM605. (blue, dashed) 95 5ROX, (green, dashed) 132 R123, (pink) 64 R560, (black, dash-dotted) 148 R6G, and (red, dotted) 71 RB molecules and immobilized on glass, presented with best-fit parameters to lognormal functions. Reprinted with permission from reference 24.

Collectively, the differences in ET kinetics represented by the lognormal fit parameters can explain the BBM accuracy of R6G/RB and the other three well performing rhodamine pairs. While the accuracy of R6G/RB classification could not be rationalized with emission intensity analysis, the off interval fit parameters of the two fluorophores are notably different. RB has a μ_{off} of –0.3 and σ_{off} of 2.6 while R6G has a μ_{off} of –1.27 and σ_{off} of 2.07. The pairs 5ROX/R6G, R6G/RB, and 5ROX/R560 also have relatively large differences in μ_{off} and σ_{off} values so, on top of emission differences, ET kinetics also reinforce their BBM classification accuracy. The remaining poorly performing pairs (aside from the formerly explained R560/RB pair) likely have overlapping kinetic and emission related properties which cause highly similar blinking-related statistics that MLR cannot discern for BBM.

Overall, binary rhodamine BBM is viable as evidenced by the 90% accuracy achieved by six pairs and the 93% accuracy possible for four pairs. This result is surprising given the shared on-off blinking mechanism but can be explained with a combination of ET kinetics and spectral properties. However, BBM can only leverage differences in recombination ET, N-dealkylation, and rotational freedom to a certain extent. Since CPD-derived blinking statistics and distributions overlap considerably, significant thresholding is necessary to achieve the 90% accuracy benchmark. Unfortunately, due to such overlapping, when extending BBM classification to three rhodamines, the average minimum average accuracy is a meager 62%. Even when elevated thresholds are applied, only the 5ROX/R6G/RB trio reaches 90% at the expense of ~85% data loss. The limitations of BBM classification with exclusively rhodamines motivates the introduction of different classes of emitters.

Exploring different emitters for BBM optimization

Successful binary classification of rhodamines shows that BBM can distinguish modest variations in blinking patterns within a shared on-off blinking mechanism. It is then predicted that introducing emitters with more structural and photophysical differences (i.e., BODIPY, anthraquinone, QD), will significantly improve binary and ternary BBM performance.

First, we investigated a BODIPY fluorophore due to their recent rise in popularity for super-resolution imaging techniques. Specifically, the BODIPY dye pyrromethene 605 (PM605) was selected for blinking analysis and BBM studies due to its 565 nm emission maximum which overlaps with the five rhodamine fluorophores **(Figure 1)**. By collecting ~100 PM605 blinking traces under the same experimental conditions and quantitatively processing via CPD, the underlying blinking mechanism of PM605 can be assessed. Unexpectedly, not only were the PM605 CPD values frequently statistically equivalent to the rhodamines (with the exception of $\langle t_{off,seg} \rangle$, $I_{min,}$ and $\langle t_{off,int} \rangle$), the associated CCDF distributions of on and off intervals were best fit to lognormal distributions and coincided with some rhodamine distributions **(Figure 3)**.[24] Therefore, it is plausible that PM605 also undergoes an Albery-type blinking mechanism such as dispersive ET. More thorough investigations of the photophysical and photochemical properties of PM506 and other BOPIPY fluorophores are underway and beyond the scope of this study.

Via MLR, PM605 was introduced into binary and ternary BBM classification problems. BBM performance showed some improvement from rhodamines alone, a promising result for the hypothesis that different classes of fluorophores can provide additional differentiability for BBM. In particular, the default binary accuracy for all rhodamine/PM605 pairs exceeds 75% **(Table 2)**. Then, when an increased threshold is applied, all pairs are capable of reaching 93% accuracy and four of five pairs maintain modest to high data retention.[24] Extending to ternary classification with two rhodamines and PM605, average minimum accuracy increases by 7.5% to 69.5% **(Figure 4)**. While default accuracy is still relatively low, 90% accuracy is possible for four combinations of two rhodamines and PM605. Even more promising, 5ROX/PM605/RB retains about 50% of its total

dataset when a 0.8 threshold is applied for 90% accurate BBM.[24] This trio represents the first viable three-fluorophore model for BBM.

Table 2: Binary BBM-based classification results with PM605, AZ, and rhodamines

Classification	minimum			for 93% accuracy	
	accuracy (%)	TPR	FPR	threshold	data retention (%)
5ROX/PM605	85.3	0.84	0.14	0.78	79
PM605/R123	82.7	0.81	0.16	0.93	40
PM605/RB	82.4	0.84	0.20	0.82	73
PM605/R560	78.9	0.83	0.28	0.88	52
PM605/R6G	76.1	0.70	0.19	0.95	12
5ROX/AZ	97.9	0.97	0.01	✓	
AZ/RB	94.5	0.96	0.08	✓	
AZ/R123	92.8	0.94	0.08	✓	
AZ/R560	87.6	0.92	0.22	0.83	77
AZ/R6G	82.3	0.82	0.17	0.79	75
AZ/PM605	74.4	0.81	0.34	0.88	29

Due to the unexpected overlap in blinking dynamics between PM605 and rhodamines, there is further opportunity to improve BBM by using emitters with more distinct blinking behavior. For instance, the organic fluorophore 1,2-dihydroxyanthriquinone, commonly known as alizarin (AZ), is capable of undergoing excited-state intramolecular proton transfer (ESIPT). ESIPT causes a broad emission band which ranges from approximately 535 to 700 nm **(Figure 1)**. At the single-molecule level, we previously noted ESIPT causes an elevated number of on segments and reduces both ET and photobleaching.[17] Due to a more distinctive blinking mechanism being operative for AZ, we expect to observe distinctive blinking statistics and/or distributions of on/off intervals which would result in higher BBM accuracy.

Indeed, AZ's unique ESIPT blinking mechanism is observed to enhance BBM performance. When paired with each of the five rhodamines, default classification accuracies range from 82.3% to an impressive 97.9% (**Table 2**). Every pair reached or exceeded 93% BBM accuracy, with the minimum data retention of 75% **(Table 2)**. When including AZ in ternary classification with two rhodamines, the average minimum accuracy now lies at 77% (**Figure 4**) with the most effective trio at the default threshold being 5ROX/AZ/R560 with an accuracy of 80.6%. The number of sets which achieve 90% accuracy with threshold increased from 4 with two rhodamines and PM605 to all 9. Further, the AZ/R123/R560 combination retains 72.3% of its dataset at this elevated accuracy.[24] However, retention at 90% accuracy can range down to 25% and data retention is consistently low when thresholding to 93% accuracy.

To further test the hypothesis that more distinctive blinking mechanism leads to better BBM performance, QDs were included in classification problems as well. QDs are semiconductor nanoparticles rather than small molecules and display brighter and more frequently fluctuating emission as well as higher photostability than R6G.[8,9,19] Additionally, previous experiments fit on and off event distributions to truncated power laws.[18,19] When QDs are included in ternary classification with two rhodamines, average minimum accuracy increases to 81.1% (**Figure 4**). Again, all 9 sets achieve 90% accuracy, now with an average retention of 72%. Even more successful are the ternary classifications with QD, AZ, and one rhodamine due to three different blinking mechanisms being operative. For these combinations, the minimum accuracy averages at 85.5% with 90% and 93% accuracy feasible for all five trios with reasonable data retention on average.[24] Indeed, the overall highest performing ternary classification was 5ROX/AZ/QD, with a default accuracy of 89.2%.[24]

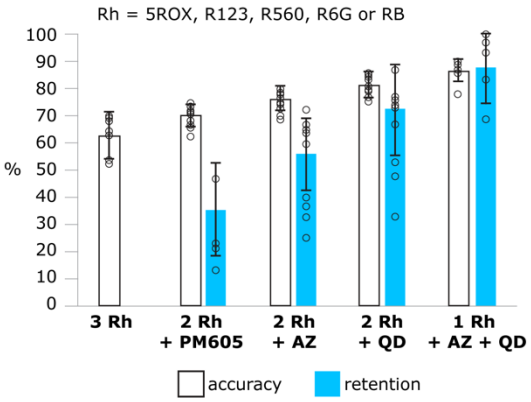

Figure 4: Bar graph summarizing the impact of structure and photophysics on average ternary BBM performance. Accuracy (white) is minimum classification accuracy and retention (blue) is average data retention corresponding to 90% classification accuracy. Reprinted with permission from reference 24.

Overall, accurate ternary BBM is accomplished across many emitter combinations, all of which are spectrally overlapped. In total, of the 39 ternary classification experiments, 19 of these sets reached 90% accuracy while retaining at least 50% of the data.[24] The trend of increasing default accuracy as well as data retention at 90% accuracy supports the interpretation that introducing different blinking

dynamics and mechanisms improves BBM performance.

CONCLUSIONS

Ultimately, BBM is capable of discerning broadly distributed and complex blinking dynamics, even when an on-off blinking mechanism is shared between fluorophores. Indeed, several pairs of the five selected rhodamines were differentiated based upon variations on emission intensities and ET kinetics within the dispersive ET framework. Hence, when considering future rhodamine probes for BBM, selecting fluorophores with differentiable ET kinetics and/or spectral diffusion tendencies would be favorable. Then, incorporating PM605, AZ, and QD, emitters with increasingly distinct photochemical and photophysical properties, results in increased BBM default classification accuracy and data retention when thresholding. Although PM605 undergoes more similar blinking dynamics to rhodamine dyes than expected, some improvement to BBM is observed and suggests BODIPY probes are a viable inclusion into BBM systems. However, modeling BBM with AZ which undergoes ESIPT and QD which employs a dispersive charge transfer process results in the highest performing two and three emitter BBM tested thus far.

By investigating the influence of emitter properties on blinking dynamics, we establish a framework for selecting fluorophores in this study and for future BBM implementations. However, some considerations will be made in future studies to address the viability of BBM for the purpose of multicolor high-resolution imaging. For instance, measurements for this study were collected using a confocal microscope, but wide field imaging is more time-effective and practical for SMLM applications. Additionally, higher labeling densities are required to implement SMLM, so the blinking of probes should be assessed at elevated densities in future studies. With these and other qualifications in mind, BBM has the potential to greatly expand the number of emitters which can be simultaneously multiplexed for SMS and SMLM applications.

ACKNOWLEDGEMENT

A.G.S acknowledges the support of the NASA Virginia Space Grant Consortium through an Undergraduate STEM Research Scholarship. This research was funded by the National Science Foundation (CHE-2102099). A.G.S also acknowledges the intellectual contributions of A.J.K., I.M.K., G.R.H., and G.A.D. and their respective funding.

REFERENCES

(1) Moerner, W. E. (William E.). Single-Molecule Spectroscopy, Imaging, and Photocontrol: Foundations for Super-Resolution Microscopy (Nobel Lecture). *Angew. Chem. Int. Ed.* **2015**, *54* (28), 8067–8093. https://doi.org/10.1002/anie.201501949.

(2) Moerner, W. E.; Orrit, M. Illuminating Single Molecules in Condensed Matter. *Science* **1999**, *283* (5408), 1670–1676. https://doi.org/10.1126/science.283.5408.1670.

(3) Tinnefeld, P.; Sauer, M. Branching Out of Single-Molecule Fluorescence Spectroscopy: Challenges for Chemistry and Influence on Biology. *Angew. Chem. Int. Ed.* **2005**, *44* (18), 2642–2671. https://doi.org/10.1002/anie.200300647.

(4) Lelek, M.; Gyparaki, M. T.; Beliu, G.; Schueder, F.; Griffié, J.; Manley, S.; Jungmann, R.; Sauer, M.; Lakadamyali, M.; Zimmer, C. Single-Molecule Localization Microscopy. *Nat. Rev. Methods Primer* **2021**, *1* (1), 1–27. https://doi.org/10.1038/s43586-021-00038-x.

(5) Patterson, G.; Davidson, M.; Manley, S.; Lippincott-Schwartz, J. Superresolution Imaging Using Single-Molecule Localization. *Annu. Rev. Phys. Chem.* **2010**, *61*, 345–367. https://doi.org/10.1146/annurev.physchem.012809.103444.

(6) Möckl, L.; Moerner, W. E. Super-Resolution Microscopy with Single Molecules in Biology and Beyond–Essentials, Current Trends, and Future Challenges. *J. Am. Chem. Soc.* **2020**, *142* (42), 17828–17844. https://doi.org/10.1021/jacs.0c08178.

(7) Jradi, F. M.; Lavis, L. D. Chemistry of Photosensitive Fluorophores for Single-Molecule Localization Microscopy. *ACS Chem. Biol.* **2019**, *14* (6), 1077–1090. https://doi.org/10.1021/acschembio.9b00197.

(8) DeSalvo, G. A.; Hoy, G. R.; Kogan, I. M.; Li, J. Z.; Palmer, E. T.; Luz-Ricca, E.; de Gialluly, P. S.; Wustholz, K. L. Blinking-Based Multiplexing: A New Approach for Differentiating Spectrally Overlapped Emitters. *J. Phys. Chem. Lett.* **2022**, *13* (22), 5056–5060. https://doi.org/10.1021/acs.jpclett.2c01252.

(9) Hoy, G. R.; DeSalvo, G. A.; Haile, S. H.; Smith, E. N.; Wustholz, K. L. Rapid, Accurate Classification of Single Emitters in Various Conditions and Environments for Blinking-Based Multiplexing. *J. Phys. Chem. A* **2023**, *127* (15), 3518–3525. https://doi.org/10.1021/acs.jpca.3c00917.

(10) Wang, L.; Frei, M. S.; Salim, A.; Johnsson, K. Small-Molecule Fluorescent Probes for Live-

Cell Super-Resolution Microscopy. *J. Am. Chem. Soc.* **2019**, *141* (7), 2770–2781. https://doi.org/10.1021/jacs.8b11134.
(11) Tan, J. A.; Rose, J. T.; Cassidy, J. P.; Rohatgi, S. K.; Wustholz, K. L. Dispersive Electron-Transfer Kinetics of Rhodamines on TiO2: Impact of Structure and Driving Force on Single-Molecule Photophysics. *J. Phys. Chem. C* **2016**, *120* (37), 20710–20720. https://doi.org/10.1021/acs.jpcc.6b01960.
(12) Wong, N. Z.; Ogata, A. F.; Wustholz, K. L. Dispersive Electron-Transfer Kinetics from Single Molecules on TiO2 Nanoparticle Films. *J. Phys. Chem. C* **2013**, *117* (41), 21075–21085. https://doi.org/10.1021/jp405899v.
(13) Kopera, K. M.; Tuckman, H. G.; Hoy, G. R.; Wustholz, K. L. Origin of Kinetic Dispersion in Eosin-Sensitized TiO2: Insights from Single-Molecule Spectroscopy. *J. Phys. Chem. C* **2021**, *125* (43), 23634–23645. https://doi.org/10.1021/acs.jpcc.1c07597.
(14) Beija, M.; Afonso, C. A. M.; Martinho, J. M. G. Synthesis and Applications of Rhodamine Derivatives as Fluorescent Probes. *Chem. Soc. Rev.* **2009**, *38* (8), 2410–2433. https://doi.org/10.1039/B901612K.
(15) Zhang, Y.; Zhang, Y.; Song, K.-H.; Lin, W.; Sun, C.; Schatz, G. C.; Zhang, H. F. Investigating Single-Molecule Fluorescence Spectral Heterogeneity of Rhodamines Using High-Throughput Single-Molecule Spectroscopy. *J. Phys. Chem. Lett.* **2021**, *12* (16), 3914–3921. https://doi.org/10.1021/acs.jpclett.1c00192.
(16) Kikuchi, K.; Adair, L. D.; Lin, J.; New, E. J.; Kaur, A. Photochemical Mechanisms of Fluorophores Employed in Single-Molecule Localization Microscopy. *Angew. Chem. Int. Ed.* **2023**, *62* (1), e202204745. https://doi.org/10.1002/anie.202204745.
(17) Tan, J. A.; Garakyaraghi, S.; Tagami, K. A.; Frano, K. A.; Crockett, H. M.; Ogata, A. F.; Patterson, J. D.; Wustholz, K. L. Contributions from Excited-State Proton and Electron Transfer to the Blinking and Photobleaching Dynamics of Alizarin and Purpurin. *J. Phys. Chem. C* **2017**, *121* (1), 97–106. https://doi.org/10.1021/acs.jpcc.6b09818.
(18) Chandrasiri, H. B.; Jing, H.; Perera, T.; Hu, Y. S.; Snee, P. T. Fluorescence Intermittency of Quantum Dot–Organic Dye Conjugates: Implications for Alternative Energy and Biological Imaging. *J. Phys. Chem. Lett.* **2023**, *14* (15), 3621–3626. https://doi.org/10.1021/acs.jpclett.3c00076.
(19) Cordones, A. A.; Bixby, T. J.; Leone, S. R. Evidence for Multiple Trapping Mechanisms in Single CdSe/ZnS Quantum Dots from Fluorescence Intermittency Measurements over a Wide Range of Excitation Intensities. *J. Phys. Chem. C* **2011**, *115* (14), 6341–6349. https://doi.org/10.1021/jp2001223.
(20) Watkins, L. P.; Yang, H. Detection of Intensity Change Points in Time-Resolved Single-Molecule Measurements. *J. Phys. Chem. B* **2005**, *109* (1), 617–628. https://doi.org/10.1021/jp0467548.
(21) Bates, W. M.; Huang, B.; Dempsey, G. T.; Zhuang, X. Multicolor Super-Resolution Imaging with Photo-Switchable Fluorescent Probes. *Science* **2007**, *317* (5845), 1749–1753. https://doi.org/10.1126/science.1146598.
(22) Zhang, Y.; Song, K.-H.; Dong, B.; Davis, J. L.; Shao, G.; Sun, C.; Zhang, H. F. Multicolor Super-Resolution Imaging Using Spectroscopic Single-Molecule Localization Microscopy with Optimal Spectral Dispersion. *Appl. Opt.* **2019**, *58* (9), 2248–2255. https://doi.org/10.1364/AO.58.002248.
(23) Chen, F.; Zhao, J.; Hidaka, H. Highly Selective Deethylation of Rhodamine B: Adsorption and Photooxidation Pathways of the Dye on the TiO 2 / SiO 2 Composite Photocatalyst. *Int. J. Photoenergy* **2003**, *5* (4), 209–217. https://doi.org/10.1155/S1110662X03000345.
(24) Seabury, A. G.; Khodabocus, A. J.; Kogan, I. M.; Hoy, G. R.; DeSalvo, G. A.; Wustholz, K. L. Blinking Characteristics of Organic Fluorophores for Blink-Based Multiplexing. *Commun. Chem.* **2024**, *7* (1), 1–12. https://doi.org/10.1038/s42004-024-01106-5.
(25) Albery, W. J.; Bartlett, P. N.; Wilde, C. P.; Darwent, J. R. A General Model for Dispersed Kinetics in Heterogeneous Systems. *J. Am. Chem. Soc.* **1985**, *107* (7), 1854–1858. https://doi.org/10.1021/ja00293a008.
(26) Riley, E. A.; Hess, C. M.; Whitham, P. J.; Reid, P. J. Beyond Power Laws: A New Approach for Analyzing Single Molecule Photoluminescence Intermittency. *J. Chem. Phys.* **2012**, *136* (18), 184508. https://doi.org/10.1063/1.4717618.